Table VI. CNDO/2 Barriers for Variation in Geometry for *trans*-Fluoropropene

	Barriers, au
Equilibrium geometry	0.0022
Displaced coordinate I	0.0021
Displaced coordinate II	0.0023

actual molecular mode under consideration has a symmetric threefold barrier. In the calculations, this mode is simulated by a rigid rotation of the methyl group. An exact calculation for a rigid rotation of the methyl group, employing the exact equilibrium geometry, should yield an upper bound to the barrier height for the actual mode. It was decided to compute the difference in the barrier for a rigid rotation of the experimentally determined, asymmetric methyl group for propylene, with respect to that for the symmetrized methyl group of the present calculations. The results of this calculation are presented in Table VII.

In summary, the results of this section indicate that the uncertainties in the geometry do not dramatically affect the accuracy of the calculated barriers. However, they do indicate that, without extensive optimization of geometry, the uncertainty in the barrier for an *ab initio* calculation may well be as much as ±0.2 kcal.

Table VII. CNDO/2 Results for Rigid Rotation of Equilibrium Asymmetric Methyl Group in Propene (0–180°)

	Total energy, au	Barrier,[a] au
Eclipsed 1	−25.7748	
Intermediate 1	−25.7738	0.0021
Staggered 1	−25.7727	
Intermediate 2	−25.7735	0.0019
Eclipsed 2	−25.7746	
Intermediate 3	−25.7737	0.0019
Staggered 2	−25.7727	

[a] CNDO/2 barrier for symmetrized coordinates employed in *ab initio* calculation is 0.0019 au.

Acknowledgments. Financial support from the Chemistry Programs, National Science Foundation Grant No. GP 8907, is gratefully acknowledged.

Molecular Motion in Spin-Labeled[1a] Phospholipids and Membranes

Wayne L. Hubbell[1b] and Harden M. McConnell*

Contribution from the Stauffer Laboratory for Physical Chemistry, Stanford University, Stanford, California 94305. *Received May 28, 1970*

Abstract: L-α-Lecithins having a paramagnetic *N*-oxyl-4′,4′-dimethyloxazolidine ring at selected positions on a fatty acid chain have been prepared. A quantitative analysis of the paramagnetic resonance spectra of these "spin-labeled" lecithins in aqueous dispersions of natural phospholipids is given in terms of an effective spin Hamiltonian that results from rapid anisotropic motions of the paramagnetic *N*-oxyloxazolidine ring. Good agreement is obtained between the observed and calculated resonance line shapes. Similar studies are presented for *N*-oxyl-4′,4′-dimethyloxazolidine derivatives of saturated fatty acids in aqueous dispersions of phospholipids and in the walking leg nerve fiber of *Homarus americanus*. The rapid anisotropic molecular motion determined from the resonance spectra can be accounted for in terms of a realistic model of rapidly interconverting isomeric states of a polymethylene chain. The analysis of the resonance data in terms of this model makes it possible to estimate the probabilities of gauche and trans conformations about carbon–carbon single bonds at various positions in fatty acid chains in phospholipid bilayers and in membranes. These calculations indicate that, for example, the fatty acid polymethylene chain in aqueous dispersions of lecithin–cholesterol (2:1 mole ratio) may be thought of as relatively "rigid rods" for a region of up to about eight carbon atoms from the fatty acid–glycerol ester linkage, with rapidly increasing probabilities for gauche states at larger distances. Similar studies with spin-labeled fatty acids bound to nerve fiber membranes indicate that the polymethylene chains on the membrane phospholipids show motional characteristics very similar to those of the 2:1 egg lecithin–cholesterol system. Qualitatively one may say that the hydrophobic regions of phospholipid bilayers and membranes become more and more "fluid" as one moves toward the terminal methyl groups of the phospholipid fatty acids.

A variety of physical techniques have been applied to the study of the structure and kinetic properties of phospholipid dispersions and membranes. Included among these techniques are, for example, X-ray diffraction, differential thermal analysis, electron microscopy, infrared spectroscopy, optical rotatory dispersion, circular dichroism, and nuclear magnetic resonance. The results of such studies have been described recently by Chapman and Wallach,[2] Levine, Bailey, and Wilkins,[3] Luzzati,[4] Lenard and Singer,[5] Robertson,[6a] Stoeckenius,[6b] and Steim, *et al.*[7]

(1) (a) Sponsored by the National Science Foundation under Grant No. GP-9315; (b) Air Force Office of Scientific Research–National Research Council Postdoctoral Fellow. This work has benefited from facilities made available to Stanford University by the Advanced Research Projects Agency through the Center for Materials Research.

(2) D. Chapman and D. F. H. Wallach in "Biological Membranes, Physical Fact and Function," D. Chapman, Ed., Academic Press, London, 1968, p 125.

(3) Y. K. Levine, A. I. Bailey, and M. H. F. Wilkins, *Nature (London)*, 220, 577 (1968).

(4) V. Luzzati in ref 2, p 71.

Phospholipids in aqueous dispersions are known to be in a bilayer configuration (see Figure 1), and this system is often used as a model for the biological membrane. Studies of even this relatively simple model have not resolved a number of important questions, some of which are considered in the present paper. The physical studies of biological membranes have been even less definitive, owing in large part to the enormous chemical complexity of these assemblages of macromolecules.

Site-directed, stable organic free radicals (spin labels) have been used to study structural and kinetic features of a number of biological macromolecules and membranes.[8-10] The present paper describes a continuation of our studies of membranes and phospholipids[11-13] and is specifically directed to the description of molecular motion in the fatty acid hydrocarbon chain region of phospholipids in dispersions and in membranes.

An intrinsic feature of the spin-label technique is that the spin-label molecules are never identical with the natural components of biological systems, and therefore they always represent some perturbation on the natural state of these systems. This difficulty can be minimized or entirely obviated by a variety of strategems, such as, for example, assay of biological function in the presence of the label and the use of labels with different structures.[10] The present paper, for example, deals with the question of the extent to which structural conclusions regarding molecular motion in the hydrocarbon region of lipid bilayers can be inferred from studies of the paramagnetic resonance of labels I, II, III(m,n), and IV(m,n).

In an early study of membranes using spin labels, Hubbell and McConnell[11] showed that the simple spin label I (2,2,6,6-tetramethylpiperidine-1-oxyl) binds to a hydrophobic region of certain membranes and undergoes a rapid and effectively isotropic motion in this hydrophobic region, with a correlation time of the order of magnitude of 10^{-10} sec. This result

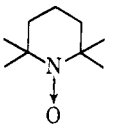

I

then led to the notion that these membrane systems contain hydrophobic regions that are locally "fluid." The great similarity of the spectrum of I in membranes and in phospholipid dispersions and the similarity in the effects of local anesthetics on these two systems[14,15] led to the conclusion that this fluid hydrophobic region in membranes is associated with the long hydrocarbon chains of the fatty acids of phospholipids.

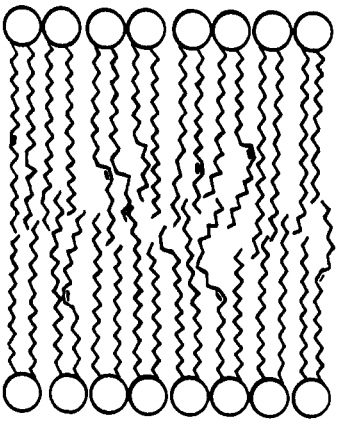

Figure 1. Schematic representation of a phospholipid bilayer. Circles represent the polar head groups and the wiggly lines the fatty acid chains.

In order to investigate further this fluid hydrophobic region of membranes, the paramagnetic resonance spectra of the following steroid and fatty acid spin labels bound to membranes as well as to phospholipid dispersions have been studied.[12,13]

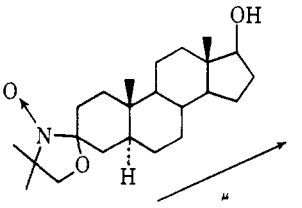

II

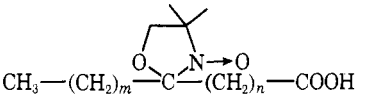

III (m,n)

It has been found that steroid and fatty acid spin labels such as II and III are oriented with their long amphiphilic axes preferentially perpendicular rather than parallel to the surfaces of certain membranes[13] or phospholipid–water interfaces.[16,17]

In neuronal membranes the steroid molecule shows rapid anisotropic motion about the amphiphilic axis μ and relatively little motion of this axis itself.[12] The paramagnetic resonance of spin labels III(12,3), III(17,3), and III(5,10) have provided an extremely interesting clue as to the nature of the structure and motion of hydrocarbon chains in membranes and phospholipid bilayers. As pointed out by Hubbell and McConnell,[13] the paramagnetic resonance spectra can be analyzed to show that the motion of the paramagnetic N-oxyloxazolidine ring in III(5,10) is far greater than this motion is in the case of III(12,3) or

(5) J. Lenard and S. J. Singer, *Proc. Nat. Acad. Sci. U. S.*, **56**, 1828 (1966).
(6) (a) J. D. Robertson, *Principles Biomol. Organ., CIBA Found. Symp., 1965*, 357 (1966); (b) W. Stoeckenius, *ibid.*, 418 (1966).
(7) J. Steim, M. Tourtellote, J. Reinert, R. McElhaney, and R. Rader, *Proc. Nat. Acad. Sci. U. S.*, **63**, 104 (1969).
(8) C. L. Hamilton and H. M. McConnell in "Structural Chemistry and Molecular Biology," A. Rich and N. Davidson, Ed., W. H. Freeman, San Francisco, Calif., 1968, p 115.
(9) O. H. Griffith and A. S. Waggoner, *Accounts Chem. Res.*, **2**, 17 (1969).
(10) H. M. McConnell and B. G. McFarland, *Quart. Rev. Biophys.*, **3**, 91 (1970).
(11) W. L. Hubbell and H. M. McConnell, *Proc. Nat. Acad. Sci. U. S.*, **61**, 12 (1968).
(12) W. L. Hubbell and H. M. McConnell, *ibid.*, **63**, 16 (1969).
(13) W. L. Hubbell and H. M. McConnell, *ibid*, **64**, 20 (1969).
(14) W. L. Hubbell, J. C. Metcalfe, and H. M. McConnell, *Brit. J. Pharm.*, **35**, 374 (1969).
(15) H. M. McConnell and W. L. Hubbell, *Proc. Int. Conf. Pharm., 4th*, 273 (1970).
(16) L. J. Libertini, A. S. Waggoner, P. C. Jost, and O. H. Griffith, *Proc. Nat. Acad. Sci. U. S.*, **64**, 13 (1969).
(17) J. C. Hsia, H. Schneider, and I. C. P. Smith, *Biochim. Biophys. Acta*, **202**, 399 (1970).

III(17,3). The spin-label results indicate that these membranes contain lipid bilayers and that the central region of the lipid bilayers is more "fluid" than is the hydrophobic region near the polar head groups.

In the present paper we give a more quantitative treatment of the resonance spectra of the fatty acid labels III(*m*,*n*); we also describe for the first time the chemical synthesis of the spin-label phospholipids IV-(*m*,*n*) and also a biradical phospholipid.

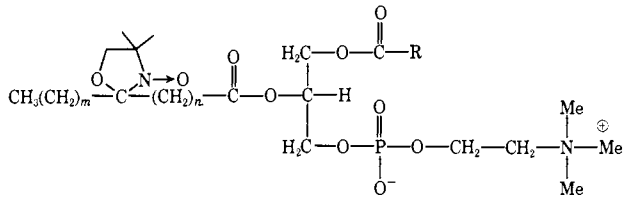

IV (*m*,*n*)

Aneja and Davies[18] recently reported the chemical synthesis of a spin-labeled phospholipid where the nitroxide group is in the polar head group region, and Keith, *et al.*,[19] have reported the biosynthetic incorporation of III(5,10) into *Neurospora* mitochondrial membrane phospholipids

Experimental Section

General Methods. Chromatographically pure egg lecithin was prepared by the method of Papahadjopoulos and Miller,[20] and stored as an ether solution under argon at −20°. For the preparation of spin-labeled dispersions of egg lecithin, the phospholipid and an appropriate amount of spin label were coated on the inner surface of a 15-ml glass tube by rotary evaporation of an ether solution. A sufficient amount of distilled water or 0.1 *M* NaCl solution was then added to make the suspension approximately 0.1 *M* in lecithin, and the tube was agitated on a vortex mixer for 60 sec.

Membranes were labeled with III(*m*,*n*) by exchange from bovine serum albumin as previously described.[12]

Electron paramagnetic resonance spectra were recorded on a Varian Associates E-4 spectrometer equipped with a variable-temperature accessory. The samples were contained in sealed Pasteur pipets.

Analytical thin layer chromatography of the phospholipids was carried out on silica gel "G" microplates prepared according to Peifer.[21] For chromatography of phosphatidic acids, the plates were exposed to the fumes of concentrated hydrochloric acid for 15 min. The chromatograms were developed with chloroform–methanol–water (65:25:4 by volume) except in the case of phosphatidic acid chromatography, where the solvent system was chloroform–methanol–hydrochloric acid (87:13:0.5 by volume). The spots were detected by charring with 50% aqueous sulfuric acid.

Crude phospholipase A was obtained as lyophilized *Crotalus adamanteus* venom (Pierce Chemical Co.); crude phospholipase D was prepared fresh from Savoy cabbage according to Davidson and Long.[22]

Infrared spectra were recorded on a Perkin-Elmer Infracord grating spectrophotometer calibrated with polystyrene film.

Preparation of III(*m*,*n*). Long-chain keto esters of the general formula $CH_3(CH_2)_mC(=O)(CH_2)_nCOOCH_3$ were prepared in excellent yield by the reaction of alkylcadmium compounds with ω-carbalkoxyacyl chlorides.[23] The ω-carbalkoxyacyl chlorides were made by the reaction of thionyl chloride with the acidic esters,[24] which in turn were made by the method of Jones[25] from the commercially available dicarboxylic acids. The 4′,4′-dimethyloxazolidine derivatives of the keto esters were prepared according to the method of Keana, *et al.*[26] Oxidation of the oxazolidine to the *N*-oxyloxazolidine with *m*-chloroperbenzoic acid, followed by alkaline hydrolysis of the ester, gave the desired III(*m*,*n*). Intermediates in the synthesis of the III(*m*,*n*) which were prepared according to well-established literature procedures were identified by their infrared spectra.

(a) III(10,3). A solution of 68.2 g of undecyl bromide (0.29 mol) in 350 ml of dry diethyl ether was added in the usual way to 6.94 g (0.29 g-atom) of magnesium turnings in 100 ml of dry diethyl ether. After the addition, the reaction was refluxed until almost complete disappearance of the magnesium.

The Grignard solution was cooled in an ice bath and 27.5 g (0.15 mol) of finely powdered anhydrous $CdCl_2$ was added in one portion. The ice bath was removed, and after a period of 30 min the ether was almost completely removed by distillation. Dry benzene (350 ml) was added and 28 g (0.23 mol) of methyl 4-(chloroformyl)butyrate (Aldrich Chemical Co.) in 100 ml of dry benzene was added over a period of 10 min with rapid stirring. The mixture was then heated to reflux for 1 hr, after which time the mixture was cooled in an ice bath and approximately 100 ml of water was added slowly with stirring. Then a large excess of 0.1 *N* sulfuric acid was added until two distinct phases formed. The benzene (upper) phase was collected and dried over anhydrous sodium sulfate. The benzene was removed under reduced pressure and the solid twice recrystallized from pentane, yielding 40 g of methyl 5-ketopalmitate: mp (uncorr) 49–50°; ir (KBr) bands at 1735 (carboxylic ester) and 1715 cm^{-1} (ketone).

To 500 ml of toluene were added 30 g (0.1 mol) of the methyl 5-ketopalmitate, 100 ml (1.0 mol) of 2-amino-2-methyl-1-propanol, and 100 mg of *p*-toluenesulfonic acid monohydrate. The mixture was refluxed for 6 days using a Dean–Stark trap for water removal. The toluene phase was then washed with six 200-ml portions of saturated sodium bicarbonate solution and four 200-ml portions of water and dried with anhydrous sodium sulfate. The toluene was removed under reduced pressure, yielding a colorless, viscous liquid. The 4′,4′-dimethyloxazolidine derivative of the methyl 5-ketopalmitate was not purified at this stage, but oxidized directly to the *N*-oxyl-4′,′4-dimethyloxazolidine derivative.

The 4′,4′-dimethyloxazolidine was dissolved in 500 ml of diethyl ether and cooled to 0° in an ice bath, and 100 ml of diethyl ether containing 22.4 g of *m*-chloroperbenzoic acid (85%, Aldrich Chemical Co.) was added over a period of 2 hr. The mixture was allowed to stand for 12 hr, at which time the ether phase was washed four times with 200-ml portions of saturated sodium bicarbonate and four times with 200-ml portions of water and dried with anhydrous sodium sulfate. The ether was removed under reduced pressure and the yellow, viscous oil chromatographed on 2 kg of silica gel, eluting with benzene–ether (7:3 v/v). The center portion of the fast-moving yellow band was collected, yielding 10 g of the *N*-oxyl-4′,4′-dimethyloxazolidine derivative of methyl 5-ketopalmitate: ir (film) band at 1735 cm^{-1} (carboxylic ester).

Anal. Calcd for $C_{21}H_{40}NO_4$: C, 68.07; H, 10.88; N, 3.78. Found: C, 68.19; H, 10.78; N, 3.73.

The nitroxide ester was dissolved in 100 ml of dioxane and 4% sodium hydroxide solution added until a precipitate began to form. When the precipitate had dissolved, more of the sodium hydroxide solution was added until another precipitate formed. This was repeated until no precipitate would form on addition of sodium hydroxide solution. The solution was brought to pH 1 with concentrated hydrochloric acid, 100 ml of water was added, and the solution was extracted with ethyl acetate. The ethyl acetate phase was dried over anhydrous sodium sulfate and the ethyl acetate removed under reduced pressure to yield the corresponding *N*-oxyl-4′,4′-dimethyloxazolidine derivative of 5-ketopalmitic acid: mp (uncorr) 45–47°, ir (KBr) band at 1710 cm^{-1} (carboxylic acid).

(b) III(7,6). This radical was prepared exactly as described for III(10,3), using 56.0 g (0.29 mol) of 1-bromooctane, 6.94 g (0.29 g-atom) of magnesium to form the Grignard, and 27.5 g (0.15 mol) of $CdCl_2$ for the exchange to the dialkylcadmium compound. The dialkylcadmium compound was treated with 50.8 g (0.25 mol) of ethyl 7-(chloroformyl)heptanoate (see (d) below for preparation). The keto ester was purified by distillation [138–138.5° (0.2 mm)] yielding 50 g of ethyl 8-ketopalmitate: mp (uncorr) 33–35°, ir (KBr) bands at 1737 (carboxylic ester) and 1718 cm^{-1} (ketone).

(18) R. Aneja and A. P. Davies, *Chem. Phys. Lipids*, **4**, 60 (1970).
(19) A. D. Keith, A. S. Waggoner, and O. H. Griffith, *Proc. Nat. Acad. Sci. U. S.*, **61**, 819 (1968).
(20) D. Papahadjopoulos and N. Miller, *Biochim. Biophys. Acta*, **135**, 624 (1967).
(21) J. T. Peifer, *Mikrochim. Acta*, 529 (1962).
(22) F. M. Davidson and C. Long, *Biochem. J.*, **69**, 458 (1958).
(23) J. Cason, *Chem. Rev.*, **40**, 15 (1947).
(24) J. Cason in "Organic Syntheses," Coll. Vol. III, E. C. Horning, Ed., Wiley, New York, N. Y., 1955, p 169.
(25) R. G. Jones, *J. Amer. Chem. Soc.*, **69**, 2350 (1947).
(26) J. W. Keana, S. B. Keana, and D. Beetham, *ibid.*, **89**, 3056 (1967).

The oxazolidine derivative was formed from 33 g (0.11 mol) of 8-ketopalmitate, 40 ml (0.55 mol) of 2-amino-2-methyl-1-propanol, and 100 mg of *p*-toluenesulfonic acid monohydrate in 500 ml of toluene.

Oxidation to the *N*-oxyl-4′,4′-dimethyloxazolidine was accomplished with 23 g of *m*-chloroperbenzoic acid (85%, Aldrich Chemical Co.) as previously described and purified by chromatography on 2 kg of silica gel, eluting with benzene–ether (7:3 v/v), yielding 8 g of the *N*-oxy-4′,4′-dimethyloxazolidine derivative of ethyl 8-ketopalmitate. The ester was hydrolyzed to the free acid as described for III(10,3), yielding a viscous orange-yellow liquid: ir (film) band at 1710 cm^{-1} (carboxylic acid).

Anal. Calcd for $C_{20}H_{38}NO_4$: C, 67.37; H, 10.74; N, 3.95. Found: C, 67.48; H, 10.74; N, 3.92.

(c) III(5,10). This radical was prepared as described by Keith, *et al.*[19]

(d) Ethyl 7-(Chloroformyl)heptanoate. Following the procedure of Jones,[25] a mixture of 88.6 g (0.5 mol) of suberic acid (Aldrich Chemical Co.), 66.7 g (0.29 mol) of diethyl suberate (Aldrich Chemical Co.), 35 ml of di-*n*-butyl ether, and 12.5 ml of concentrated HCl was heated under reflux for 0.5 hr, 30 ml of 95% ethanol added, and heating continued for 2 hr. An additional 10 ml of 95% ethanol was added, the mixture was boiled under reflux for 2 more hr, and the water and dibutyl ether were distilled under vacuum. The remaining hot liquid was poured into 1.5 l. of petroleum ether and allowed to stand at 20° for 1 hr, after which the precipitated suberic acid was removed by filtration. The filtrate was extracted with a total of 1 l. of 0.4 *M* sodium bicarbonate solution. The combined aqueous extracts were acidified with concentrated hydrochloric acid and extracted with three 200-ml portions of diethyl ether. After drying over anhydrous sodium sulfate, the ether was removed under reduced pressure and the remaining liquid distilled under vacuum to yield 61.9 g of ethyl hydrogen suberate: ir (film) bands at 1700 and 1730 cm^{-1} (carboxylic acid and ester, respectively).

The ethyl hydrogen suberate (61.9 g, 0.3 mol) and 47.6 g (0.4 mol) of thionyl chloride were warmed to 40° for 3 hr in a 250-ml round-bottom flask fitted with a reflux condenser. The flask was then left to stand at room temperature for 6 hr. The excess thionyl chloride was distilled off with a Claisen head and the acid chloride distilled under vacuum, yielding 63 g of ethyl 7-(chloroformyl)-heptanoate: ir (film) bands at 1730 (carboxylic ester) and 1780 cm^{-1} (acyl halide).

Preparation of IV(*m*,*n*). (a) III(*m*,*n*) Anhydrides. The III(*m*,*n*) anhydrides were prepared by the following general method of Selinger and Lapidot.[27]

To 75 ml of dry carbon tetrachloride containing 10 mmol of III(*m*,*n*) was added 1.03 g (5 mmol) of dicyclohexylcarbodiimide in 25 ml of dry carbon tetrachloride. After 12 hr, the precipitated dicyclohexylurea was removed by filtration through sintered glass and the carbon tetrachloride removed under reduced pressure. The anhydrides were used without further purification: ir (CCl_4) bands at 1810 and 1750 cm^{-1} (carboxylic anhydride).

(b) Egg Lysolecithin. To 1 g of egg yolk lecithin in 300 ml of ether was added 50 mg of lyophilized *Crotalus adamanteus* venom (Pierce Chemical Co.) in 4 ml of 5 m*M* $CaCl_2$ solution. At the end of 1.5 hr, 100 ml of ethanol was added and the volume reduced under vacuum to about 25 ml. The remaining solution was centrifuged at low speed to remove the precipitated enzyme. The precipitate was washed once with 2:1 v/v chloroform–methanol and the extract combined with the original supernatant. The volume was reduced to approximately 2 ml and this added to 40 ml of diethyl ether. The precipitated lysolecithin was collected by centrifugation and washed twice with 40 ml of diethyl ether.

(c) Acylation of Egg Lysolecithin with III(*m*,*n*) Anhydrides. The method used here is due to Cubero Robles and Van den Berg[28] and is illustrated by the acylation of egg lysolecithin with III(10,3) anhydride.

To 50 mg (approximately 0.1 mmol) of egg lysolecithin in a 10-ml pear-shaped flask was added 0.27 g (0.39 mmol) of III(10,3) anhydride and 3 mg (0.05 mmol) of finely powdered sodium oxide. The flask was sealed and slowly rotated in an oil bath at 60°. Periodically, the reaction mixture was examined by thin layer chromatography. A gradual increase in the amount of lecithin was observed with a concomitant decrease in the lysolecithin, which had completely disappeared after 24 hr. A small amount (0.5 ml) of $CHCl_3$ was then added to the reaction mixture and the resulting solution applied to 7 g of Unisil (Clarkson Chemical Co., Williamsport, Pa.) which had been activated for 12 hr at 120°. The fatty acids and excess anhydride were eluted with 2% methanol in chloroform, leaving a yellow band at the origin. The methanol content was then increased in 5% increments up to 40% methanol in chloroform and the yellow band collected. Evaporation of the solvent yielded 40 mg of a waxy yellow solid. The thin layer chromatographic behavior of the lecithins prepared by this method (IV-(10,3), IV(7,6), and IV(5,10) lecithins) was nearly identical with that of natural egg lecithin.

The spin-labeled lecithins were hydrolyzed by phospholipase A to yield the corresponding III(*m*,*n*) acid and a compound which cochromatographed with natural lysolecithin. Phospholipase D degradation gave a new compound which behaved on thin layer chromatography like authentic phosphatidic acid.

It should be noted that while the IV(5,10) lecithin was hydrolyzed by both enzymes at approximately the same rate as natural lecithin, the IV(7,6) and IV(10,3) lecithins were hydrolyzed at a much slower rate, the effect being largest with phospholipase A.

The ir spectra of the lecithins were consistent with published spectra of synthetic lecithins,[28] with bands at 1735, 1075, and 1250 cm^{-1} (solid film).

(d) Acylation of L-α-Glycerophosphorylcholine by III(7,6) Anhydride. Acylation of L-α-glycerophosphorylcholine was accomplished by the method of Cubero Robles and Van den Berg.[28]

The crystalline cadmium chloride complex of L-α-glycerophosphoryl choline (Sigma Chemical Co., St. Louis, Mo.) was converted to free L-α-glycerophosphorylcholine by the method of Baer and Kates.[29]

To a 10-ml pear-shaped flask was added 27.3 mg (approximately 0.1 mmol) of L-α-glycerophosphorylcholine, 71.3 mg (0.2 mmol) of III(7,6), and 2.0 ml of 0.1 *N* NaOH (0.2 mmol). The solution was lyophilized and the residue dried at 40° for 48 hr. To this was added 0.278 g (0.4 mmol) of III(7,6) anhydride and the flask was rotated slowly at 60° for 2 days. Purification was as described for the IV(10,3) lecithin, yielding 20 mg of pure material which behaved on thin layer chromatography like natural lecithin.

The compound was hydrolyzed by phospholipase A to yield the III(7,6) acid and a compound which behaved like natural lysolecithin on thin layer chromatography.

Degradation with phospholipase D yielded a compound which behaved like authentic phosphatidic acid on thin layer chromatography. The hydrolysis by both enzymes was much slower than that of natural egg lecithin.

The ir spectrum is consistent with published spectra for synthetic lecithins,[28] having bands at 1735, 1075, and 1250 cm^{-1} (solid film).

Analysis of Electron Paramagnetic Resonance Spectra

In this section we show how it is possible to obtain a quantitative understanding of the paramagnetic resonance spectra of spin labels III(*m*,*n*) and IV(*m*,*n*) in phospholipid bilayer systems.

Except for unresolved proton hyperfine structure, the paramagnetic resonance spectra of nitroxide radicals with spin $^1/_2$ having fixed orientations in crystals can be accounted for with high accuracy with the basic spin Hamiltonian, $\mathcal{H}$[10]

$$\mathcal{H} = |\beta|S\cdot\mathbf{g}\cdot\mathbf{H} + h\mathbf{S}\cdot\mathbf{T}\cdot\mathbf{I} - g_N\beta_N\mathbf{I}\cdot\mathbf{H} \qquad (1)$$

Here **H** is the applied field vector, **g** and **T** are the electronic g-factor and hyperfine tensors, β and β_N are the electron and nuclear Bohr magnetons, and h is Planck's constant. **S** and **I** are the electron and nuclear spin angular momentum operators in units of $\hbar$. The elements of **g** and **T** in eq 1 vary slightly from one nitroxide radical to another and also depend slightly on the polarity of the solvent.[8] The nitroxide radicals discussed in the present work are all *N*-oxyl-4′,4′-dimethyloxazolidine (NODO) derivatives of ketones. We have determined the elements of $\mathcal{H}$ in eq 1 for the NODO derivative of 5-α-cholestan-3-one, when present

(27) Z. Selinger and Y. Lapidot, *J. Lipid Res.*, 7, 174 (1966).

(28) E. Cubero Robles and D. Van den Berg, *Biochim. Biophys. Acta*, 187, 520 (1969).

(29) E. Baer and M. Kates, *J. Amer. Chem. Soc.*, 70, 1394 (1948).

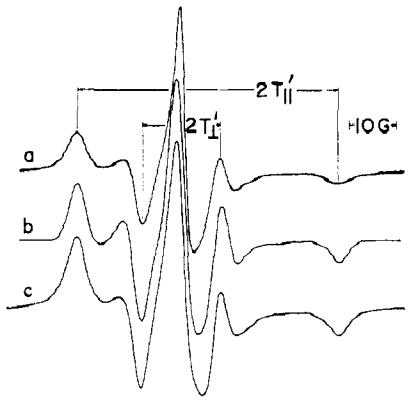

Figure 2. Paramagnetic resonance spectra of the phospholipid spin label IV(10,3) (see text) in an aqueous dispersion of egg lecithin–cholesterol (2:1 mole ratio): (a) observed spectrum, (b) calculated spectra using Gaussian line shape, (c) calculated spectra using Lorentzian line shape.

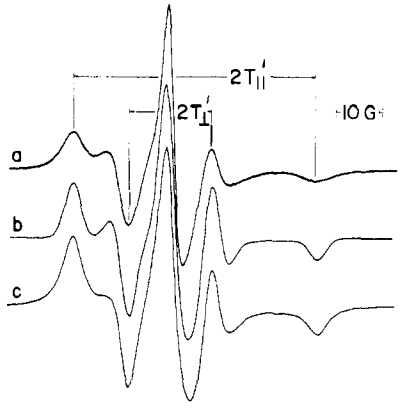

Figure 3. Paramagnetic resonance spectra of the phospholipid spin label IV(7,6) (see text) in an aqueous dispersion of egg lecithin–cholesterol (2:1 mole ratio): (a) observed spectrum, (b) calculated spectra using Gaussian line shape, (c) calculated spectra using Lorentzian line shape.

as substitutional impurities (~1%) in single crystals of cholesteryl chloride. Cholesteryl chloride forms a

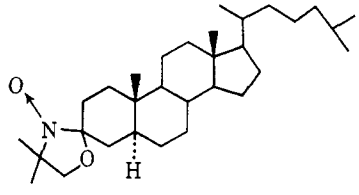

V

monoclinic lattice with two molecules per unit cell.[30] Single crystals containing V in cholesterol chloride were grown by crystallization from ether–ethanol solutions containing about one molecule of the label per hundred of the chloride. The principal axis z was found to be parallel to the unique crystalline b axis. The analysis of the single-crystal spectra is given elsewhere.[31] The parameters obtained for the spin Hamiltonian are

$$(g_x, g_y, g_z) = (2.0089, 2.0058, 2.0021 \pm 0.001) \quad (2)$$

$$(T_x, T_y, T_z) = (16.2, 16.2, 86 \pm 2 \text{ Mc}) \quad (3)$$

$$= (5.8, 5.8, 30.8 \pm 0.5 \text{ G})$$

(30) J. D. Bernal, D. Crowfoot, and I. Fankuchen, *Phil. Trans. Roy. Soc. London, Ser. A*, 239, 135 (1946).
(31) W. L. Hubbell, Thesis, Stanford University, 1969.

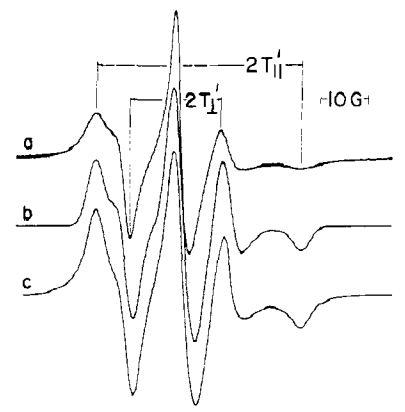

Figure 4. Paramagnetic resonance spectra of the phospholipid spin label IV(5,10) (see text) in an aqueous dispersion of egg lecithin –cholesterol (2:1 mole ratio): (a) observed spectrum, (b) calculated spectra using Gaussian line shape, (c) calculated spectra using Lorentzian line shape.

In every case studied thus far it has been found that the principal axes of **g** and **T** coincide.[10]

Spin labels such as II and III often show paramagnetic resonance spectra in phospholipid and membrane systems that can be interpreted in terms of rapid anisotropic motion.[13] In many cases we have found that the observed spectra can be accounted for in terms of an effective Hamiltonain $\mathcal{H}'$, as follows.

In the presence of molecular motion, the spin Hamiltonian in eq 1 becomes time dependent, since the tensors **g** and **T** are molecule fixed and the field direction **H** is laboratory fixed. This time-dependent Hamiltonian $\mathcal{H}(t)$ can always be divided into two parts, an effective time-independent Hamiltonian $\mathcal{H}'$, and a time-dependent Hamiltonian $\{\mathcal{H}(t) - \mathcal{H}'\}$.

$$\mathcal{H}(t) = \mathcal{H}' + \{\mathcal{H}(t) - \mathcal{H}'\} \quad (4)$$

The effective Hamiltonian $\mathcal{H}'$ has the form

$$\mathcal{H}' = |\beta|\mathbf{S}\cdot\mathbf{g}'\cdot\mathbf{H} + h\mathbf{S}\cdot\mathbf{T}'\cdot\mathbf{I} - g_N\beta_N\mathbf{I}\cdot\mathbf{H} \quad (5)$$

Here the elements of $\mathbf{g}'$ and $\mathbf{T}'$ are suitable averages of the elements of **g** and **T**. The utility of the decomposition in eq 4 depends on the extent to which the observed spectra can be accounted for by the effective Hamiltonian $\mathcal{H}'$. For spin labels such as II and III, this is often the case, as described below. For these labels *rapid anisotropic* molecular motion is responsible for the fact that the observed spectra can be accounted for in terms of a time-independent Hamiltonian $\mathcal{H}'$. The motion *must* be *anisotropic* if $\mathcal{H}'$ contains anisotropic terms, and the motion must be rapid enough so that the time-dependent fluctuations in $\{\mathcal{H}(t) - \mathcal{H}'\}$ can be neglected. Let us now assume that for a given case the Hamiltonian $\mathcal{H}'$ arises from rapid anisotropic molecular motion and *does* account for the observed paramagnetic resonance spectra of a given label in a given environment. Let the principal axes of $\mathcal{H}$ and $\mathcal{H}'$ be x, y, z and x', y', z', respectively. Suppose a strong field **H** is applied in the principal axis direction z'. In this case the spin components $S_{z'}$ and $I_{z'}$ are good quantum numbers, and the energy in terms of the effective Hamiltonian $\mathcal{H}'$ is simply

$$E = |\beta|g_{z'z'}'S_{z'}H_{z'} + hT_{z'z'}S_{z'}I_{z'} - g_N\beta_N I_{z'}H_{z'} \quad (6)$$

In terms of the basic Hamiltonian the energy is

$$E = |\beta|(\overline{\alpha^2}g_{xx} + \overline{\beta^2}g_{yy} + \overline{\gamma^2}g_{zz})S_{z'}H_{z'} + h(\overline{\alpha^2}T_{xx} + \overline{\beta^2}T_{yy} + \overline{\gamma^2}T_{zz})S_{z'}I_{z'} - g_N\beta_N I_{z'}H_{z'} \quad (7)$$

Here α, β, and γ are the direction cosines of z' in the x, y, z principal axis system, and $\overline{\alpha^2}$, $\overline{\beta^2}$, and $\overline{\gamma^2}$ are the time averages of the squares of these direction cosines, the averages being over the rapid anisotropic molecular motion. From eq 6 and 7 it follows that

$$g_{z'z'}' = \overline{\alpha^2}g_{xx} + \overline{\beta^2}g_{yy} + \overline{\gamma^2}g_{zz} \quad (8)$$

$$T_{z'z'}' = \overline{\alpha^2}T_{xx} + \overline{\beta^2}T_{yy} + \overline{\gamma_2}T_{zz} \quad (9)$$

Since T_{xx} and T_{yy} are (accidentally) equal for the NODO ring, and since $\alpha^2 + \beta^2 + \gamma^2 = 1$, eq 9 may be written in the simplified form

$$T_{z'z'}' = a + {}^2/_3(T_{zz} - T_{xx})S \quad (10)$$

Here a is the isotropic component of the hyperfine

$$a = {}^1/_3\mathrm{Tr}(\mathbf{T}) \quad (11)$$

$$= {}^1/_3\mathrm{Tr}(\mathbf{T}') \quad (12)$$

interaction and S is an "order parameter"[32]

$$S = {}^1/_2(3\overline{\gamma^2} - 1) \quad (13)$$

The adequacy of the effective Hamiltonian $\mathcal{H}'$ can be demonstrated by comparison of observed and calculated spectra derived from the eigenstates of $\mathcal{H}'$. Comparisons of observed and calculated spectra are given in Figures 2, 3, and 4 for phospholipid spin labels IV(10,3), IV(7,6), and IV(5,10) in egg lecithin–cholesterol (2:1 mole ratio) dispersions in water. The computer program is similar to the one used by Itzkowitz for "strongly immobilized" spectra.[33] The agreement between the experimental and calculated spectra is good but not perfect As far as we can tell, the principal discrepancy in each case can be attributed to the line-shape input parameter in the theoretical calculation, which is known to be imperfect (see below). The calculated spectra are based on an axially symmetric effective spin Hamiltonian, with hyperfine interactions, $T_{||}'$, $T_{\perp}'$, and g factors, $g_{||}'$, $g_{\perp}'$, parallel and perpendicular to the symmetry axis. The values of these parameters used for calculating the spectra in Figures 2, 3, and 4 are given in Table I. In principle,

Table I. Resonance Data[a] for Phospholipid Spin Labels IV(m,n) in Egg Lecithin–Cholesterol (2:1 Mole Ratio)

Spin label	$T_{||}'$	$T_{\perp}'$	a'	$g_{||}' - g_{\perp}'$	S
IV(10,3)	27.8	9.0	15.2	−0.0036	0.695
IV(7,6)	26.0	9.5	15.0	−0.0033	0.62
IV(5,10)	21.8	10.3	14.1	−0.0026	0.46

[a] $T_{||}'$, $T_{\perp}'$, and a' are in gauss.

the "best" values for the parameters of the effective spin Hamiltonian can be determined by varying these parameters, and the resonance line-shape parameter, until the differences between observed and calculated spectra are minimized. The imput parameters of the spectral calculations are $T_{||}'$, $T_{\perp}'$, $g_{||}' - g_{\perp}'$, and the line width and line shape. These can be determined, or estimated, as described below.

(1) Values of $T_{||}'$ were determined by measuring the separation of the outer hyperfine extrema and equating this separation to $2T_{||}'$, as indicated in Figures 2, 3, and 4.[13]

(2) The outer signals in Figures 2, 3, and 4 are separated by $2T_{||}'$, and are expected to have, to a good approximation, the *line shapes of the absorption curves* for a perfectly oriented ensemble of radicals with the applied field parallel to the symmetry axis, even though the spectra in these figures are derivative curve presentations of resonance spectra of an isotropic distribution of radical orientations. The experimentally observed outer signals have line shapes that are sometimes almost perfectly Lorentzian but are sometimes intermediate between Lorentzian and Gaussian. Thus, the outer signals provide at least approximate line-width and line-shape parameters for the numerical spectral calculation.

(3) Values of the hyperfine splitting perpendicular to the symmetry axis, $T_{\perp}'$, can be estimated[13] from the separation of the inner hyperfine extrema, as illustrated in Figures 2, 3, and 4, where the inner hyperfine extrema are separated by $2T_{\perp}'$. More accurate values for $T_{\perp}'$ can be obtained from observed spectra by the method described later.

(4) Values of the spectroscopic splitting factors, $g_{||}'$ and $g_{\perp}'$, can be estimated directly from the observed spectra: $g_{||}'$ can be determined from the center point of the outer hyperfine extrema, and $g_{\perp}'$ from the center point of the inner hyperfine extrema. As discussed later, values of $g_{||}' - g_{\perp}'$ determined using this center-point method may have an intrinsic error of *ca.* 5–10% for spectra of the type described here.

Calculated spectra are given in Figures 2, 3, and 4 using Lorentzian as well as Gaussian line shapes. The line-width parameters used for these calculated spectra were chosen so as to optimize the overall agreement between the experimental and calculated spectra. In the spectra where the low-field outer hyperfine extrema are well resolved, the half-height line widths of the outer lines are 4.6 (Figure 2) and 5.5 G (Figure 3). In the calculated spectra in Figures 2 and 3 Lorentzian half-height line widths of 5.1 G were used. Thus, in these cases it is reasonable to pick a line-width parameter from the outer low-field hyperfine extremum. The Gaussian line shapes that give the best overall agreement between the observed and calculated spectra have half-height line widths of 3.7 G, which differs significantly from the observed low-field hyperfine extrema in Figures 2 and 3 (4.6 and 5.5 G). This evidence, as well as the line shapes of the outer hyperfine extrema, suggests that Lorentzian line shapes are more appropriate for these calculations.

The agreement between observed and calculated spectra is good, but not perfect. We suspect that a principal source of the remaining discrepancy arises from line broadening due to heterogeneity in the fatty acid chains of the lecithin host.

It is evident from the above discussion that the line positions, and also line shapes, of the outer hyperfine extrema play an important role in the analysis of the

(32) A. Saupe, G. Englert, and A. Pova, *Advan. Chem. Ser.*, **No. 63**, 51 (1965).

(33) M. Itzkowitz, Thesis, California Institute of Technology, 1966; *J. Chem. Phys.*, **46**, 3048 (1967).

resonance spectra. We present here a simple demonstration that to a good approximation the outer hyperfine extrema are indeed separated by $2T_{||}'$ and that the *derivative curve presentations* of these outer hyperfine extrema for an isotropic distribution of label orientations give line shapes that correspond to the absorbtion curve of a perfectly oriented array of labels with the applied field **H** parallel to the principal axes z' of the effective Hamiltonian $\mathcal{H}'$.

The resonance absorption due to transitions between the eigenstates of $\mathcal{H}'$ has three components: the low- (high-) field extremum arises from eigenstates such that when $S_z = {}^1/_2$, the component of nuclear spin angular momentum in the local field direction is $m = 1$ (-1). The central hyperfine component of the spectra arises from eigenstates where $m = 0$. The resonance absorption spectra of nitroxide radicals having fixed orientations in single crystals have been studied extensively. In the angular region $0 \leq \vartheta \leq$ 60–70°, the resonance line positions for each hyperfine component m can be represented to a good approximation by the equation[10]

$$H_r^{(m)}(\vartheta,\varphi) = H_0^{(m)}(1 - \lambda_m \cos \vartheta) \qquad (13.1)$$

Here ϑ and φ are the polar and azimuthal angles giving the field direction in the principal axis system x, y, z or, when appropriate, x', y', z'. $H_r^{(m)}(\vartheta,\varphi)$ is the position of the resonance line for the low-field hyperfine line ($m = 1$), the central hyperfine line ($m = 0$), and the high-field hyperfine line ($m = -1$).

Let the paramagnetic resonance absorption spectrum due to the hyperfine state m be $a_m(\xi)$, where $\xi = H - H_r^m(\vartheta,\varphi)$. In the simplest cases, a_m is a Gaussian or Lorentzian function of ξ with a line-width parameter that is independent of ϑ and φ. This contribution to the total absorption spectrum due to component m is

$$A_m(H) = \int_{\vartheta=0}^{\vartheta=\pi/2} a_m(\xi) \sin \vartheta d\vartheta \qquad (13.2)$$

The corresponding contribution to the derivative curve spectrum is

$$\frac{\partial A_m}{\partial H} = \int_{\vartheta=0}^{\vartheta=\pi/2} \frac{\partial a_m(\xi)}{\partial \xi} \sin \vartheta d\vartheta \qquad (13.3)$$

If ξ is now approximated by the expression for $H_r^{(m)}(\vartheta,\varphi)$ in eq 13.1, we see that the resulting derivative curve spectrum will be accurate in the region $0 \leq \vartheta \leq$ 60–70°, and inaccurate outside this region. The result of the integration indicated in eq 13.3 is simply

$$\frac{\partial A_m}{\partial H} = \frac{1}{H_0^{(m)}\lambda_m}[a_m(H - H_0(1 - \lambda_m)) - a_m(H - H_0)] \qquad (13.4)$$

The first term on the right-hand side of eq 13.4 is the $\vartheta = 0$ absorption curve, and the second term is a (negative) absorption curve corresponding to radicals oriented with $\vartheta = \pi/2$. However, this latter contribution to $\partial A_m/\partial H$ is erroneous since the approximation in eq 13.1 is incorrect when $\vartheta \simeq \pi/2$. The first term is valid and corresponds to the absorption curve for radicals for which $\vartheta = 0$. The same arguments apply to the effective Hamiltonian $\mathcal{H}'$; the analysis clearly breaks down if, for example, the two curves $a_m(H - H_0(1 - \lambda_m))$ and $a_m(H - H_0)$ overlap one another, or if approximation eq 13.1 is not valid for the range of ϑ corresponding to the line width of a_m. For nitroxide radicals, line shapes for the hyperfine component $m = 0$ cannot be obtained from eq 13.4 for both of these reasons.

A discussion similar to that given above, but restricted to Gaussian line shapes, has been given earlier by McConnell and McFarland.[10] Also, it should be noted that Searl, Smith, and Wyard[34] have been able to obtain an analytic expression for the derivative of the absorption spectrum for an isotropic distribution of principal axis orientations, where each orientation gives a Lorentzian absorption curve. Unfortunately, the line-position function $H_r(\vartheta,\varphi)$ considered by these authors is not applicable to the present problem. A significant difference between the case considered by Searl, *et al.*, and that considered above is that in our case the peaks of the "parallel" hyperfine extrema are expected to determine $2T_{||}$ (and $g_{||}$) with high accuracy. This has been verified for all our calculated spectra when the outer hyperfine extrema do not overlap seriously with the inner hyperfine resonance signals.

In discussing the molecular motion of spin labels in phospholipids and membranes, the order parameter S and $\overline{\alpha^2} - \overline{\beta^2}$ are of particular interest. Equations 10 and 12 can be combined to yield the following expression for S

$$S = \frac{T_{||}' - T_{\perp}'}{T_{zz} - T_{xx}} \qquad (14)$$

This simple equation can then be used to determine S from $T_{||}'$, $T_{\perp}'$, T_{zz}, and T_{xx} in the case that the effective Hamiltonian $\mathcal{H}'$ has axial symmetry and that T_{xx} and T_{yy} are (accidentally) equal. For axial symmetry, the following equation relates $g_{||}' - g_{\perp}'$ to S and $\overline{\alpha^2} - \overline{\beta^2}$

$$g_{||}' - g_{\perp}' = [g_{zz} - {}^1/_2(g_{xx} + g_{yy})]S + {}^3/_4(g_{xx} - g_{yy})(\overline{\alpha^2} - \overline{\beta^2}) \qquad (15)$$

Unfortunately, the evaluation of *accurate* values for the order parameter S using eq 14 is not straightforward.[35] It is known that there is a small dependence of the isotropic hyperfine interaction a of nitroxide radicals on solvent polarity.[8] For example, the isotropic hyperfine interaction is 14.1 G for the NODO ring in V in hexane. The value of a calculated for the isotropic hyperfine interaction from the single-crystal data (*cf.* eq 3 and 11) is also 14.1 G, as expected for the hydrophobic environment in the crystal. The isotropic hyperfine interaction observed in the resonance of II in distilled water is 15.2 G. Thus, it is necessary that the numerator and denominator in eq 14 refer to the same solvent polarity, whereas the values of T_{xx} and T_{zz} in eq 3 clearly refer to a hydrophobic environment. The polarity of the local environment for the nitroxide group in III(m,n) or IV(m,n) can be assessed from the isotropic hyperfine interactions a' calculated from eq 12. Values for a' for the phospholipids IV(m,n) are given in Table I. It is clear that the environment of the NODO ring is "polar" at positions $n = 3$ and $n = 6$, and nonpolar or hydrophobic at position $n = 10$. Since both the isotropic and anisotropic terms

(34) J. W. Searl, R. C. Smith, and S. J. Wyard, *Proc. Phys. Soc., London*, 74, 491 (1959).
(35) J. Seelig, *J. Amer. Chem. Soc.*, 92, 3881 (1970).

in the spin Hamiltonian are approximately proportional to the spin density on nitrogen, and it is the spin density that is doubtless dependent on solvent polarity, we assume that the ratio of the isotropic and anisotropic interactions is constant irrespective of solvent polarity. Thus, if T_{zz} and T_{xx} in eq 3 are used in the calculation of S, then the corrected expression for S is

$$S = \left(\frac{T_{\parallel}' - T_{\perp}'}{T_{zz} - T_{xx}}\right)\left(\frac{a}{a'}\right) \qquad (16)$$

The values of S given in Table I have been calculated using eq 16. The interpretation of these values of S in terms of molecular motion of fatty acid chains is given in the next section.

At present there is no accurate information on the dependence of the elements of the **g** tensor on solvent polarity. In the study of the resonance spectra of III(m,n) in smectic liquid crystals,[35] only a negligible variation in Tr(**g**′) was found for n in the range $2 \leq n \leq 10$. If we make the assumption that the elements of **g**′ also have no strong dependence on solvent, then the elements of **g** given in eq 2 may be used along with the observed S to estimate $\overline{\alpha^2} - \overline{\beta^2}$ using eq 15. The calculated spectra given in Figures 2, 3, and 4 use **g**′ tensors based on the values of the **g** tensor given in eq 2, together with eq 15 and the assumption that $\overline{\alpha^2} = \overline{\beta^2}$. The values of $g_{\parallel}' - g_{\perp}'$ taken from the experimental curves, from the calculated spectra using Gaussian line shape functions, and from the calculated spectra using Lorentzian functions are all identical to within experimental error. These values of $g_{\parallel}' - g_{\perp}'$ are calculated using the center-point method described earlier in item 4. We conclude that the value of $g_{\parallel}' - g_{\perp}'$ used for the spectral calculation and given in Table I must be accurate to *ca.* 2%. (This does *not* mean that a value of $g_{\parallel}' - g_{\perp}'$ estimated by the center-point difference method of item 4 is accurate to 2%, but rather that the value of $g_{\parallel}' - g_{\perp}'$ estimated from the center-point difference method is proportional to the exact value of $g_{\parallel}' - g_{\perp}'$ and that this value is obtained from the numerical calculation that gives the best fit to the spectra. The values of $g_{\parallel}' - g_{\perp}'$ estimated from the center-point difference method typically differ from the exact values of $g_{\parallel}' - g_{\perp}'$ by *ca.* 5–10%.) An error of 2% or less in $g_{\parallel}' - g_{\perp}'$ signifies that $\overline{\alpha^2} - \overline{\beta^2} = 0$ to within ± 0.03.

Values of $T_{\perp}'$ can also be estimated from the observed spectra when $2T_{\perp}'$ is taken equal to the separation of the peaks shown in Figure 2. As judged by the calculated spectra, this determination of $T_{\perp}'$ typically yields a result which is too small by *ca.* 0.8 G. Thus, for spectra with axial symmetry such as those shown in Figures 2, 3, and 4, more accurate values of $T_{\perp}'$ can be obtained directly from the observed spectra by making this correction when $T_{\perp}'$ is in the range 4–12 G.

When the effective Hamiltonian $\mathcal{H}'$ does *not* have axial symmetry, it is usually not possible to determine $T_{x'x'}'$ and $T_{y'y'}'$ from the observed spectra because of overlapping resonance lines (at least for applied fields of 3000 G). In this case one can only estimate the order parameter, using eq 10, and reasonable estimates of the appropriate values of a, T_{zz}, and T_{xx} to be used. It should be emphasized that the polar–hydrophobic corrections to a, T_{zz}, and T_{xx} are only crucial when accurate values of S are required. Unfortunately, in the absence of axial symmetry, one does not have the checks on self-consistency in the spectral interpretation that one does in the case of axial symmetry. The outer signals (separated by $2T_{z'z'}'$) should be well resolved; otherwise the use of eq 10 to calculate an order parameter, or even the use of an effective Hamiltonian $\mathcal{H}'$, may not be justified.

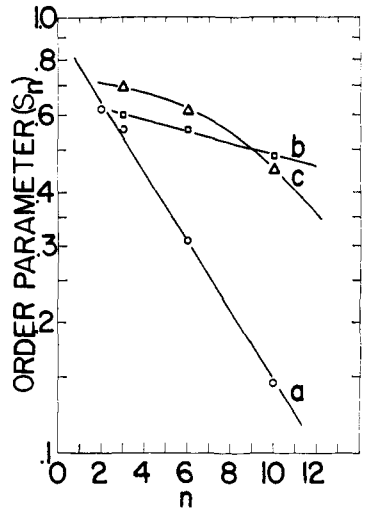

Figure 5. The order parameter S_n for (a) fatty acid spin labels III(m,n) (see text) in smectic liquid crystals of decanol–sodium decanoate (data of Seelig, ref 35), (b) fatty acid spin labels III(m,n) in aqueous dispersions of egg lectihin–cholesterol (2:1 mole ratio), (c) phospholipid spin labels IV(m,n) (see text) in aqueous dispersion of egg lecithin–cholesterol (2:1 mole ratio).

Molecular Motion in Phospholipid Bilayers and Membranes

Figure 5 gives a semilog plot of the order parameter S_n *vs.* n, where n is the number of methylene groups in IV(m,n) and III(m,n) that separate the paramagnetic NODO ring from the carbonyl group, when these labels are incorporated into aqueous dispersions of egg lecithin–cholesterol (2:1 mole ratio). Also included in Figure 5 are the data of Seelig[35] showing the order parameters for the fatty acids III(m,n) in oriented smectic liquid crystals.

Two of the plots in Figure 5 indicate that the order parameter S_n depends exponentially on n. For example, log S_n is approximately a linear function of n for III(m,n) in smectic liquid crystals and phospholipid–cholesterol dispersions. Even though this simple exponential dependence of S_n on n does not hold for the important phospholipid spin labels IV(m,n), a simple exponential dependence of S_n on n is nevertheless of considerable interest from a theoretical point of view, and serves as a useful starting point for more elaborate treatments of molecular motion in bilayers.

Seelig has shown that the Porod–Kratky model for a methylene chain leads to an exponential dependence of S_n on n.[35] This model assumes free rotation about each carbon–carbon bond, the angle between adjacent carbon–carbon single bonds being an adjustable parameter. One end of the chain, the carboxyl group, is "anchored" or rigidly fixed at the bilayer–water interface. However, it is known that the Porod–Kratky model is a poor representation of the physical

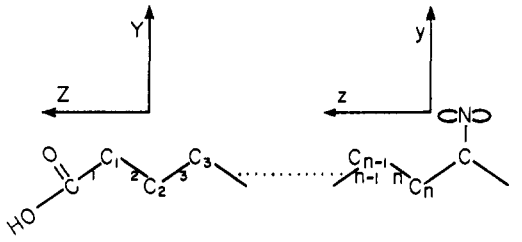

Figure 6. Spin label III(m,n) fatty acid in extended (all trans) conformation. The Z axis is parallel to the chain direction. The principal hyperfine axis z is perpendicular to the N-oxyloxazolidine ring, parallel to the π-orbital axis that holds the odd electron, and also parallel to Z when the polymethylene chain is extended. Carbon atoms and bonds are numbered as indicated.

properties of polymethylene polymers,[36] so it is clearly desirable to see whether a more accurate description of the isomeric states of polymethylene chain also leads to an exponential dependence of S_n on n. We show here that under certain conditions a realistic description of the isomeric conformational states of a polymethylene chain, anchored at one end, does lead to an exponential dependence of S_n on n.

Consider a long-chain fatty acid whose polymethylene chain is extended in the Z direction, as sketched in Figure 6. In this fully extended conformation of the polymethylene chain, the principal hyperfine axis z is parallel to Z. Gauche–trans isomerizations about the various carbon–carbon bonds between the NODO ring (located on the carbon atom numbered $n + 1$ in our numbering scheme) bring about a fluctuation in the angle between z and Z. Isomerizations that are rapid compared to anisotropies in the hyperfine interaction lead to the average effective Hamiltonian $\mathcal{H}'$.

The principal axis of $\mathcal{H}'$, that is z', is known to be perpendicular to the bilayer surface for III(m,n) in the homogeneously oriented smectic liquid crystal system studied by Seelig.[35] It is also known for IV(5,10) that z' is preferentially perpendicular rather than parallel to the bilayer surface in phospholipid multilayers[16] and in membranes.[13] It is also clear from the work of Hubbell and McConnell[13] and Seelig[35] that the order parameter S_n for labels III(m,n) depends strongly on n and only weakly on m.

The theoretical calculation of S_n as a function of n is easily carried out under the following assumptions. (1) All carbon–carbon bonds in the polymethylene chain are equivalent to one another in the sense that the *a priori* probabilities of gauche$^+$ or gauche$^-$ conformation is so small that one can neglect the statistical probabilities of states having gauche conformations about adjacent carbon–carbon bonds. (Adjacent gauche$^+$ gauche$^-$ conformations have very low thermodynamic probabilities at ordinary temperatures owing to steric hinderance.[36]) (3) The rapid *axial* motion of the steroid label II in phospholipid bilayers and membranes[12] makes it extremely likely that there is a comparably rapid axial motion for III(m,n).

Let P_t be the probability that any single carbon–carbon bond be in a trans conformation, and P_g be the probability that any carbon–carbon single bond be in a gauche (either gauche$^+$ or gauche$^-$) conformation. $P_g + P_t = 1$. Then the order parameter S_n may be approximated by the following equation

$$S_n = P_t^n\eta_0 + nP_t^{n-1}P_g\eta_1 + \frac{n(n-1)}{2!}P_t^{n-2}P_g^2\eta_2 + \ldots \quad (17)$$

In eq 17, P_t^n is the probability that the methylene chain be all trans between the carboxyl group and the NODO group and $nP_t^{n-1}P_g$ is the probability that this chain will have one gauche conformation, etc. The use of these binomial probabilities is of course only adequate if in the real chain the gauche probabilities are so small that there is little chance of having adjacent gauche conformations. Otherwise we would have to exclude explicitly those terms in eq 17 that correspond to energetically unfavorable conformations. In eq 17, η_0 ($=1$) is the value of $\frac{1}{2}(3\overline{\gamma^2} - 1)$ when the chain is all trans and fully extended, η_1 ($= -\frac{1}{8}$) is the value of $\frac{1}{2}\cdot(3\overline{\gamma^2} - 1)$ when the chain has one gauche$^+$ bond for half the time and one gauche$^-$ bond for half the time and is otherwise fully extended (all trans). In the expansion in eq 17, η_2 represents the average value of $\frac{1}{2}(3\overline{\gamma^2} - 1)$ when the methylene chain contains *two* gauche bonds, equal weight being given to g^+g^+, g^-g^-, g^+g^-, and g^-g^+ isomeric states, and to isomeric states in which the gauche bonds are separated by even and odd numbers of carbon atoms. Values of η_n for $n > 2$ are defined in a similar way, assuming equal probabilities for even and odd numbers of carbon atoms separating bonds in gauche conformations. The calculated values of η_n decrease in magnitude with increasing n; $\eta_2 = \frac{1}{16}$, $\eta_3 = -\frac{1}{32}$. These values for the η_n were obtained by direct calculation; the details are not given here since the calculations are straightforward but tedious.

We see from eq 17 that in general S_n is *not* a simple exponential function of n; however, the values of η_n for $n > 0$ are so small that for sufficiently large values for P_t, S_n is very nearly a simple exponential function. Let us rewrite eq 17 as follows

$$\log S_n - C = n \log P_t \quad (18)$$

$$C = \log\left\{\eta_0 + n(P_g/P_t)\eta_1 + \frac{n(n-1)}{2!}(P_g/P_t)^2\eta_2 + \ldots\right\} \quad (19)$$

In cases where plots of log S_n *vs.* n give straight lines, values of P_t are easily obtained from eq 18 and 19 by an iteration procedure. Thus, when C is neglected in eq 18, the linear plot of log S_n *vs.* n yields a first estimate for P_t, say P_t'. This value of P_t' is inserted in eq 19 to obtain C', and then a plot of log $S_n - C'$ *vs.* n is used to obtain a second approximation to P_t, say P_t''. For example, consider the data of Seelig for the fatty acid labels III(13,2), III(12,3), II(9,6) and III(5,10) in decanol–sodium octanoate liquid crystals.[35] The plot of log S_n *vs.* n yields $P_t' = 0.82$, $P_g' = 0.18$, and the first iteration obtained by plotting log $S_n - C'$ *vs.* n yields $P_t'' = 0.85$, $P_g'' = 0.15$. The convergence is evidently rapid for the series in eq 17 (and 19). This rapid convergence is due in large part to the fact that the η_n decrease rapidly with increasing n. This rapid convergence is in contrast to the rather slow convergence of the binomial

(36) P. J. Flory, "Statistical Mechanics of Chain Molecules," Interscience, New York, N. Y., 1969.

expansion itself

$$1 = P_t^n + nP_t^{n-1}P_g + \frac{n(n-1)}{2!}P_t^{n-2}P_g^2 + \ldots \quad (20)$$

When, for example, $P_t = 0.85$ and $n = 10$, the leading term on the right-hand side of (20) is only $(0.85)^{10} \simeq 0.145$.

When the probability of an all-trans conformation is only 14.5%, we may question the legitimacy of neglecting interactions between certain gauche conformations (such as, for example, adjacent g^+g^- conformations). However, even for $n = 10$, $P_t = 0.85$, the number of forbidden adjacent gauche$^+$gauche$^-$ conformations which should be omitted from eq 17 (and 19) and is not is only *ca.* 10% of the total number of isomers included in the calculation.

As a second example, consider the order parameters S_n for the fatty acids III(m,n) bound to dispersions of egg lecithin–cholesterol. Here the slope of the log S_n *vs.* n plot yields a value for the trans probability P_t of 0.976. This trans probability signifies that in a chain of, say, 15 carbon–carbon single bonds, the probability of the all-trans conformation is *ca.* 70%.

It will be noted that in general the linear plots of log S_n *vs.* n do not pass through the point log $S_0 = 0$, $n = 0$. In the case of the smectic liquid crystal data the correction of log S_n by C in eq 18 *does* lead to a straight line passing through the point $n = 0$, log $S_0 = 0$. However, this is definitely *not* the case for the fatty acid labels in the 2:1 egg lecithin–cholesterol dispersions. The simplest explanation is that these fatty acid spin labels have a rapid, anisotropic rigid-body motion superimposed on the gauche–trans isomerizations discussed above. Indeed, it is known from an earlier study by Hubbell and McConnell[12] that the rigid steroid spin label II undergoes a rapid anisotropic motion in phospholipid bilayers and in membranes. Since spin labels III(m,n) are approximately "straight rigid sticks" ($P_t = 0.976$) in 2:1 egg lecithin–cholesterol dispersions, we may assume that the preferred direction of the rigid stick axis Z is parallel to the preferred chain direction of the surrounding lipids. If the *instantaneous* direction of Z is not perpendicular to the bilayer surface, then rapid rocking motions of Z can be expected to produce a reduction of the order parameter over and above that due to gauche–trans isomerizations. If we assume that the amplitude of this rapid anisotropic rigid stick motion is independent of the state of gauche–trans isomerization of the polymethylene chain, then this additional motion can be taken into account in eq 17 and 18 by including a factor S_0 which is the average of $\frac{1}{2}(3\cos^2\theta - 1)$ for the rigid straight stick motion, where θ is the angle between the axis of the rigid stick (which is parallel to z when the chain is extended) and z'.

$$S_n = S_0(P_t^n\eta_0 + nP_t^{n-1}P_g\eta_1 + \ldots) \quad (21)$$

$$\log S_n - \log S_0 - C = n \log P_t \quad (22)$$

For the fatty acid spin labels III(m,n) in 2:1 egg lecithin–cholesterol dispersions, $S_0 = 0.64$. It is very important to emphasize that this result is quite consistent with the *possibility* that the probable instantaneous orientation of the principal hyperfine axis z (or the rigid stick methylene chain axis) is *not* perpendicular to the bilayer surface, even though the principal axis of the effective Hamiltonian $\mathcal{H}'$ may be perpendicular to the bilayer surface.

Finally, we consider the order parameters S_n for the phospholipid labels IV(m,n) in 2:1 egg lecithin–cholesterol dispersions, given in Figure 5. Here a plot of log S_n *vs.* n deviates markedly from linearity. There are two general mechanisms that could give rise to this deviation. First, if the nature of the chain segmental motion were such that the direction of the principal axis z' of the effective Hamiltonian depended on chain position n, then one would expect deviations from the simple exponential decrease of S_n. Second, since the gauche, trans probabilities P_g, P_t already depend strongly on the environment (host) of the spin-labeled fatty acid chain, one expects that in general the gauche and trans probabilities depend to some extent on chain position n. We shall tentatively assume that this second explanation of the curvature in Figure 5 is correct, particularly for $n > 4$. In that case, values of P_g and P_t at various chain positions can be estimated from the following equation, which follows from a simple generalization of eq 21 but takes advantage of the fact that the leading term in the equation is dominant when $P_t > 0.85$.

$$\frac{S_n - S_{n+1}}{S_n} = (P_g)_{n+1} \quad (23)$$

Support for the validity of our model, as well as for the transferability of the values of P_g, P_t from the spin labels to the fatty acid chains in phospholipid bilayers, is given in the next section.

We have observed the paramagnetic resonance spectra of the 1,2-di-III(7,6) lecithin biradical in various phospholipid dispersions. In the more fluid systems, the paramagnetic resonance line shapes of the biradical are very similar to those of the corresponding III(7,6) monoradical, indicating only weak magnetic spin–spin interactions. This result can be understood by considering the low probability that all $2n$ carbon–carbon bonds are in the all-trans configuration, where the odd electrons are doubtless close enough to one another to produce a detectable interaction. For example, data are presented in the next section that show that the trans probabilities, P_t, for carbon–carbon bonds in dipalmitoyllecithin, at temperatures just above the phase transition, are equal to *or less than* 0.89. Thus the probability that both chains be extended (presumably parallel) is less than $(0.89)^{12} \simeq 0.26$ for this biradical. At temperatures below the phase transition, there is a marked broadening of the resonance lines, due to spin–spin interaction. In oriented, multilayer films, the line widths are found to be anisotropic. A detailed line-shape analysis will be required to extract quantitative information on the spin–spin distribution function.

Mesomorphic Phase Transitions in Phospholipids

Phospholipids exhibit a large variety of phases, which depend on the chemical composition of the phospholipid, relative concentrations of water and phospholipid, and temperature.[3,37] Of particular interest here is the strong endothermic phase transition exhibited by fully hydrated lecithins containing saturated fatty acid

(37) B. D. Ladbrooke and D. Chapman, *Chem. Phys. Lipids*, 3, 304 (1969).

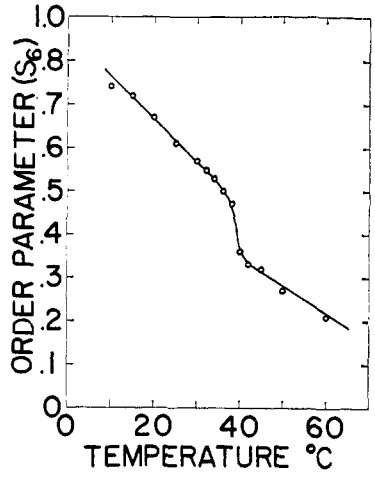

Figure 7. Plot of the order parameter S_6 for phospholipid spin label IV(7,6) present to the extent of 1 mol % in an aqueous dispersion of dipalmitoyllecithin, as a function of temperature.

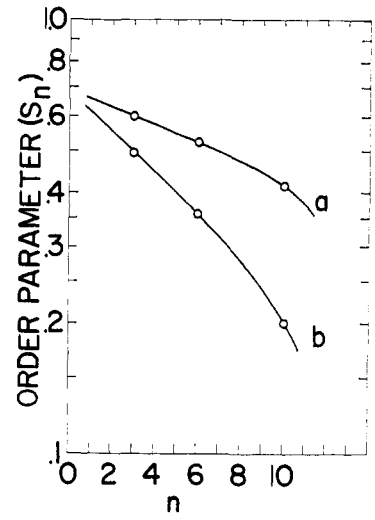

Figure 8. The order parameter S_n as a function of n for phospholipid spin labels IV(m,n) (see text) in aqueous dispersions of dipalmitoyllecithin (a) 4° below and (b) 1° above the transition temperature, 39°.

chains.[38] This transition has been studied extensively by Phillips, Williams, and Chapman[38] and has been attributed to a "melting" of the polymethylene chains. The transition is sometimes described as the "α crystalline gel at maximum hydration → liquid crystal at maximum hydration"; we shall refer to this phase transition as "the" phase transition.

The phase transitions in a series of saturated lecithins show heats of transition that are linearly related to the number of methylene groups in the fatty acid chains.[38] From these heats one can calculate the configurational entropy of transition per carbon–carbon bond, for bonds that are 14–22 carbon atoms from the ester carbonyl group. This configurational entropy of transition, Δs, is 1.25 cal deg^{-1} mol^{-1} of carbon–carbon bonds. If we assume that this transition is one between states of the hydrocarbon chain that are essentially fully extended ($P_t \simeq 1$, $P_g \simeq 0$) to one in which there is appreciable population of the gauche states, then we may estimate P_t and P_g in the melted liquid crystal state by the formula

$$\Delta s = P_t \ln P_t + P_g \ln (P_g/2) \qquad (24)$$

(This equation neglects repulsive interactions between adjacent $g^{\mp}g^{\mp}$ conformations and is only accurate when P_g is small.[36]) Equation 24 leads to $P_t = 0.80$, $P_g = 0.20$. It will be noted first of all that these thermodynamic values of P_t and P_g are close to those we derived above from the data of Seelig for the fatty acid labels III(m,n) in the decanol–sodium octanoate liquid crystals. These thermodynamic probabilities P_t, P_g cannot of course be compared with these probabilities for spin labels III(m,n) or IV(m,n) in the 2:1 egg lecithin–cholesterol host bilayer system, since the egg lechithin contains unsaturated fatty acid chains (which decrease P_t and increase P_g relative to saturated chains) and cholesterol (which increases P_t and decreases P_g relative to saturated chains). A direct comparison between the thermodynamic data and the resonance data is obtained by a study of the resonance spectra of spin labels IV (m,n) in dipalmitoyllecithin (DPL)–H_2O, where the endothermic phase transition occurs at approximately 40°. A plot of S_n *vs.* temperature shows the phase transition as an abrupt decrease in S_n at 39° for each of the IV(m,n) labels in DPL–80% water. Figure 7 shows a plot of S_6 *vs.* temperature for the label IV(7,6) in DPL–80% water.

Semilog plots of S_n *vs.* n are given in Figure 8 for two temperatures, one just above the transition temperature and one just below the transition temperature. In the range of n where log S_n is a linear function of n ($3 \leqslant n \lesssim 8$), we estimate an entropy of 0.43 cal deg^{-1} mol^{-1} below the transition and 0.82 cal deg^{-1} mol^{-1} above the transition. The configurational entropy of transition is then estimated to be 0.39 cal deg^{-1} mol^{-1} of carbon–carbon single bonds, for single bonds between $n = 3$ and $n \sim 8$. This of course is considerably less than the 1.25 cal deg^{-1} mol^{-1} obtained from the thermodynamic data for $10 < n < 20$. However, it can be seen from the data in Figure 5, as well as Figure 8, that P_g increases rapidly for $n > 7$–8. Unfortunately, the resonance spectra that are needed to calculate the order parameters and configurational entropies are just those that are the most difficult to analyze since $T_{\parallel}'$ does not differ greatly from $T_{\perp}'$. Our best estimates of S_n for IV(5,10) are given in Figure 8 and are based on comparisons between experimental spectra and computer-simulated spectra similar to those given in Figures 2, 3, and 4. For $n = 10$, we estimate that the configurational entropy is 0.58 cal deg^{-1} mol^{-1} below the transition and 1.12 cal deg^{-1} mol^{-1} above it, leading to a higher transition entropy, 0.54 cal deg^{-1} mol^{-1}. Judging from the shapes of the S_n *vs.* n curves, even higher transition entropies for larger n are to be expected, and might well approach the value of 1.25 cal deg^{-1} mol^{-1} obtained from the thermodynamic data.

The spectra of IV(m,n) in phospholipid dispersions, both DPL and egg lecithin containing cholesterol, *indicate* that the hydrocarbon chains in the region $3 < n < 8$ are quite tightly packed, whereas as n increases beyond 8, these hydrophobic regions become rapidly more fluid.

A comparison of the resonance spectra of spin labels I, II, III(m,n), and IV(m,n) in aqueous dispersions of DPL through the transition temperature is of interest in

(38) M. C. Phillips, R. M. Williams, and D. Chapman, *Chem. Phys. Lipids*, 3, 234 (1969).

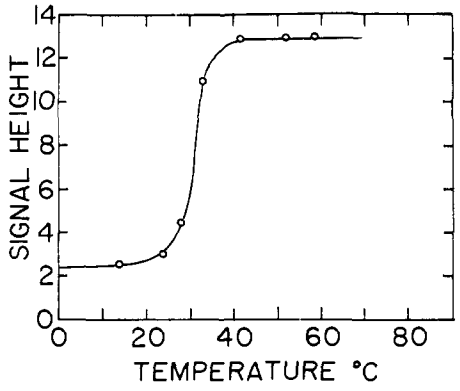

Figure 9. Paramagnetic resonance intensity of 3,4-dihydro-2,2,6,6-tetramethylpiperidine-1-oxyl in the fluid hydrophobic region of dipalmitoyllectithin (data of Horwitz, ref 39). Because of overlapping resonance lines, the signal height does not approach zero at the lower temperatures, as it should. Similar results are obtained with spin label I (see text).

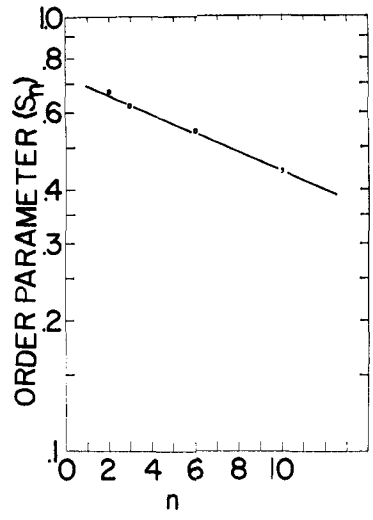

Figure 10. The order parameter S_n for spin labels III(m,n) in the walking leg nerve fiber of the Maine lobster, *Homarus americanus*.

connection with the question as to whether spin labels overly perturb the system under investigation. As already discussed, labels IV(m,n) show resonance spectra that faithfully indicate the normal transition temperature of DPL–H_2O and moreover show changes in order parameters S_n that are doubtless qualitatively and probably quantitatively the same as those appropriate to the pure phospholipid. In an early study of membranes using the spin label I, the solubility of this label in the hydrophobic region of the membranes was taken to indicate the presence of highly fluid regions in these membranes. In Figure 9 we give data obtained in this laboratory by Horwitz[39] showing the solubility of I in the hydrophobic regions of DPL–H_2O dispersions as a function of temperature. Here again the resonance spectrum of the label faithfully reveals the transition and the presence of a "fluid" hydrophobic region above the transition temperature. The resonance of II in the DPL–H_2O system also shows a marked decrease of motional freedom below the transition temperature. Still another nitroxide radical has been found by Barrett, Green, and Chapman to show this transition.[40] A study of the resonance spectra of III(m,n) in the DPL–H_2O system as a function of temperature shows a complication not encountered with Labels I, II, and IV(m,n) discussed above. No sharp change in the resonance spectra (or S_n) is observed when DPL–80% water is doped with III(10,3) at a mole ratio of III(10,3):DPL of 1:600. However, if this ratio is increased to 1:100, then a sharp decrease in S_3 is observed at 37°. The explanation of this peculiar result is by no means clear at present. In general terms, the large spectral change may be brought about when the concentration of III(10,3) exceeds its solubility in the DPL–gel phase, perhaps somewhat analogous to the results obtained for label I. However, a detailed study of the phase diagram may be necessary to understand this concentration dependence of the resonance of III(10,3) in DPL as a function of temperature.

Spin Labels in Membranes

One ultimate goal of studies using spin labels such as I, II, III(m,n), and IV(m,n) is to investigate membrane structure, particularly the structure and dynamics of the lipids in membranes. Many, but certainly not all, models of membrane structure postulate a lipid bilayer such as the one depicted in Figure 1 as an essential ingredient of the membrane. Thus, the classical Danielli–Davson model postulates a lipid bilayer coated on each side with protein.[5] Other models of membranes propose complex intertwined mesh works of lipid and protein.

In our studies of membranes using labels, we have not only found fluid-like hydrophobic regions in both membranes and bilayers, but in studies of spin labels III(m,n) bound to a number of different biological membranes, we have consistently found increasing motion (decreasing S_n) with increasing n.[18,41] That is, the binding sites for labels III(m,n) in the biological membranes are those where the hydrophobic region becomes more and more fluid as one moves away from the polar head group region, as judged by the resonance spectra of the labels. This result, coupled with the known preferred direction of III(m,n) in axonal and erythrocyte membranes indicates to us that at least some biological membranes must contain bilayer or bilayer-like regions. The purpose of the present section is simply to show briefly how quantitative information on gauche–trans probabilities for III(m,n) can be obtained in a biological membrane system, the unmyelinated walking leg axon nerve fiber of the Maine lobster, *Homarus americanus*.

Figure 10 shows a semilog plot of S_n *vs.* n for III(m,n) in these axonal membranes. The slope yields a value of $P_t = 0.96$, a value considerably higher than that obtained for III(m,n) in egg lecithin dispersions, but quite close to the value obtained with 2:1 egg lecithin–cholesterol. Studies of IV(m,n) in membranes have not yet been carried out (see later), but judging from the results in the phospholipid dispersions, we conclude that the motion of the III(m,n) chain provides at least a crude indication of the motions of the fatty acid chains on the membrane phospholipids. In any case, the conformational limits of the III(m,n) chain is dictated by its local environment, and the values of P_t determined for the III(m,n) chain give a feeling for the "rigidity" of

(39) A. F. Horwitz, Thesis, Stanford University, 1970.
(40) M. D. Barrett, D. K. Green, and D. Chapman, *Chem. Phys. Lipids*, 3, 140 (1969).
(41) S. Rottem, W. L. Hubbell, L. Hayflick, and H. M. McConnell, *Biochim. Biophys. Acta*, **219**, 104 (1970).

that environment. Thus, the hydrocarbon chains on membrane phospholipids can be thought of as nearly rigid rods ($P_t \sim 0.96$), at least for the regions where $n < 10$.

Results of experiments on membranes labeled with IV(m,n) must be interpreted with caution, since membrane preparations have the enzymatic capacity to degrade phospholipids. Our experiments with phospholipases A and D indicate, however, that these enzymes degrade IV(10,3) and IV(7,6) very slowly relative to natural lecithin, while degradation of IV(5,10) is nearly as rapid as that for the natural substrate. Use of IV(m,n) with $n < 6$ as membrane labels may then overcome the anticipated problem of *in vivo* degradation.

Structure and Reactivity in the Vapor-Phase Photolysis of Ketones. XV. Methyl Cyclopropyl Ketone[1a-c]

Dana G. Marsh[1d] and J. N. Pitts, Jr.*

Contribution from the Department of Chemistry, University of California, Riverside, California 92502. *Received April 24, 1970*

Abstract: The vapor-phase photochemistry of methyl cyclopropyl ketone has been reinvestigated. Methyl cyclopropyl ketone undergoes a Norrish type I split to yield carbon monoxide and radical fragments at 3130 and 2537–2654 Å. Methyl cyclopropyl ketone also photoisomerizes *via* a π^*-assisted cyclopropane fission to yield methyl *cis*-propenyl ketone, methyl *trans*-propenyl ketone, and methyl allyl ketone in a primary process. The quantum yields for carbon monoxide and the three photoisomers formed in a primary process in the photolyses of methyl cyclopropyl ketone vary with temperature, pressure, and wavelength, but are independent of light intensity. The results of quenching experiments at 2537–2654 Å with TME (2,3-dimethyl-2-butene), molecular oxygen, and nitric oxide and with piperylene at 3130 Å indicate that the reactions are occurring from the first excited *singlet* state of methyl cyclopropyl ketone. Furthermore, the pressure, temperature, and wavelength dependence of the quantum yields suggests that the products arise from vibrationally excited levels of this first excited singlet state.

The vapor-phase photochemistry of methyl cyclopropyl ketone was first reported by Pitts and Norman in 1954,[1a] who identified the major primary product as methyl propenyl ketone. It was reported that methyl *cis*-propenyl and methyl *trans*-propenyl ketones were formed, but their relative amounts were not determined. They reported in detail upon the formation of secondary radical products.

The efficiency of the temperature-independent (25–120°) rearrangement ($\Phi = 0.3$) of methyl cyclopropyl ketone to methyl propenyl ketone compared to free radical and carbon monoxide production ($\Phi = 0.1$) suggested the use of the cyclopropyl group as a "structural probe" in aliphatic ketone series to investigate energy transfer from the excited carbonyl group (n,π^*) to the cyclopropyl ring.[1b,c]

This paper presents detailed studies on the photoisomers formed from methyl cyclopropyl ketone in *primary* processes and the nature of the excited state involved. A mechanistic interpretation of the results is given.

Experimental Section

Apparatus and Procedure. The photochemical apparatus consists of a medium-pressure mercury-arc ultraviolet light source, a system of filters to isolate narrow-wavelength regions of the ultraviolet spectrum, an optical quartz reaction chamber and pumping system, two RCA 935 photodiodes utilized in a Wheatstone bridge circuit for measurements of relative radiant energy, a Toepler pump and gas buret system for quantum yield and actinometric determinations, and a conventional high-vacuum system for handling gases and liquids.

A Hanovia Type A medium-pressure mercury arc was used for all analytical studies. The lamp was mounted in a water- and air-cooled housing. The lamp was operated at 500 W (150 V and 3.3 A) by an inductance-stabilized 165-V output transformer, with input voltage provided by a Sola 1000-W ac voltage stabilizer. When used in this arrangement the lamp was quite stable, the light intensity varying less than 3% over a period of months.

Two wavelength regions were used during the study. A Jena Glaswerk 3130-Å interference filter system was used for longer wavelength studies, whereas a 4.5-cm-path chlorine vapor filter (at 1 atm) in series with a 2-mm-path Corning 7-54 (red-purple Corex) were used for the 2537–2654-Å region.

Quartz lens systems were used to collimate and focus the light such that a parallel beam of light completely illuminated the quartz reactor vessel and impinged upon the RCA 935 photodiode. A portion of the incident light is reflected off a quartz plate set at about 45° into another RCA 935 photodiode. These photodiodes are employed in two arms of a Wheatstone bridge circuit. When a high-sensitivity galvanometer is used as a nulling device, this arrangement allows the measurement of small fractions of absorbed light (corresponding to low-pressure runs) with an uncertainty less than 2%.

The quartz reactor vessel (2.5 × 20 cm) was contained within a cylindrical aluminum furnace, the temperature of which could be varied between room temperature and 350° and automatically controlled to within 2% at any temperature. The reactor vessel was contained in a closed loop with an all-glass pumping device which continuously circulates starting material and reaction products. This pumping and short photolysis times (low chemical conversions) serve to minimize or eliminate unwanted secondary reactions.

Quantum yield measurements for the formation of carbon monoxide and methane and actinometric determinations were made using a combination Toepler pump–gas buret assembly. The top of the gas buret was modified such that samples could be withdrawn in sample stopcocks and mass spectral or gas chromatographic determinations could be made. Starting ketone and prod-

(1) (a) Paper I, J. N. Pitts, Jr., and I. Norman, *J. Amer. Chem. Soc.*, **76**, 4815 (1954); (b) paper IV, L. D. Hess and J. N. Pitts, Jr., *ibid.*, **89**, 1973 (1967); (c) paper V, L. D. Hess, J. L. Jacobson, K. Schaffner, and J. N. Pitts, Jr., *ibid.*, **89**, 3684 (1967); (d) taken from the doctoral dissertation of D. G. Marsh, University of California, 1969.